Figure legends

Figure 1. Inducible expression of VGLUT1 in osteoclasts.
(**A**) RT-PCR analysis of brain, osteoblasts, MC3T3-E1 (clonal osteoblasts), MC3T3-G2/PA6 (clonal stroma cell line from calvariae), ST2 (clonal stroma cell line from bone marrow), C3H10T1/2 (clonal fibroblast cell line), osteoclasts, RAW264.7 macrophages and RAW264.7 cells treated with RANKL. The arrowhead indicates the VGLUT1 transcript. (**B**) VGLUT2 and VGLUT3 genes were not detectable in bone cells. Results of RT-PCR analysis of total cellular RNA are shown. Expression of G3PDH gene is also shown as a control. (**C**) Northern blotting revealing expression of the VGLUT1 gene in mature osteoclasts and RAW264.7 cells treated with RANKL. The G3PDH transcript, as a loading control, is also shown (lower panel). (**D**) Western blotting reveals the presence of VGLUT1 in RAW264.7 cells treated with RANKL. The presence of V-ATPase subunit *A* on the same blot is also shown. (**E)** RAW264.7 cells were cultured in the presence of RANKL for the indicated incubation periods (days) and the expression of VGLUT1 during osteoclastogenesis was observed by immunohistochemistry. Negative control with control IgG was also shown in insets. Bar = 10 μm. (**F**) Osteoclasts (OC) in femora of VGLUT1$^{+/+}$ (wild type) mice visualized by TRAP staining (red) contain VGLUT1, which was visualized by the HRP-DAB method (charcoal). No VGLUT1 immunoreactivity was seen in osteoclasts from VGLUT1$^{-/-}$ mice. Bar = 10 μm.

Figure 2. Immunohistochemical localization of VGLUT1 in bone-resorbing osteoclasts. Osteoclasts were grown on pieces of bone. Localization of VGLUT1 was examined by double-labeling immunofluorescence microscopy. The staining pairs were as follows: VGLUT1 and actin (A), VGLUT1 and tubulin (B), VGLUT1 and lysobisphosphatidic acid (6C4) (C), and VGLUT1 and cathepsin K (D), and VGLUT1 and fluorescent bone degradation products (E), respectively. The immunological localization was observed under a confocal microscope. A horizontal view of a merged picture is also shown. Bar = 10 μm.

Figure 3. Double gold labeling immunoelectronmicroscopy of bone-resorbing osteoclasts. Arrows and arrowheads indicate VGLUT1 (10 nm in diameter) and bone degradation product (5 nm in diameter), respectively. (A) VGLUT1-containing small vesicles; (B) vesicles containing both VGLUT1 and bone degradation products localized near the basolateral region; (C) vesicles containing bone degradation products but little VGLUT1 localized near the ruffled border membrane. Bar = 100 nm.

Figure 4. VGLUT1-mediated vesicular storage of L-glutamate.
(**A**) Time course of L-glutamate uptake by membrane vesicles isolated from RAW264.7 cells treated with or without RANKL determined in the presence or absence of ATP. n = 3. **(B)**. Effects of various compounds on the ATP-dependent L-glutamate uptake by membrane vesicles of RAW264.7 cells treated with RANKL for 1 week. Additions: bafilomycin A_1, 1 μM; CCCP, 1 μM; Evans blue, 1 μM; D, L-aspartate, 10 mM; KCl, 100 mM. In some experiments, KCl was substituted with K-acetate or omitted from the assay medium. The results are shown as means ± SEM, n = 4.

Figure 5. Regulated secretion of L-glutamate and fluorescent bone degradation products from RAW264.7 cells treated with RANKL. (**A**) RAW264.7 cells treated with RANKL or RAW264.7 cells (2.0×10^5 cells/dish) were stimulated with 50 mM KCl. The L-glutamate released was measured. (**B)** L-glutamate secretion after 20 min is shown. In some experiments, cells were treated for 2 h with 1 μM bafilomycin A_1, 50 μM EGTA-AM, or 10 μM nocodazole, and then stimulated with KCl. (**C**) Fluorescent bone degradation products in the medium under the conditions in **B** were assessed fluorometrically. The results are means ± SEM, n = 4. Asterisks indicate statistically significant numbers (* $p < 0.01$, ** $p < 0.001$). ATP stimulates the secretion of L-glutamate (**D**) and fluorescent bone degradation products (E) from RAW264.7 cells treated with RANKL. The assay was

started by the addition of 1 mM ATP. In some experiments, 0.1 mM PPADS was also included. The results are means ± SEM, n = 4. Asterisks indicate statistically significant numbers (* $p < 0.01$, ** $p < 0.001$).

Figure 6. Both KCl- and ATP-dependent L-glutamate secretion were impaired in osteoclasts from VGLUT1$^{-/-}$ mice. The time course of KCl-dependent L-glutamate secretion from osteoclasts (2.0×10^5 cells/dish) prepared from bone marrow of wild type VGLUT1$^{+/+}$ (**A**), VGLUT1$^{+/-}$ (**B**) or VGLUT1$^{-/-}$ (**C**) was measured as in Figure 5 in the presence (open squares) or absence (closed squares) of 50 mM KCl. (**D**) In osteoclasts (2.0×10^5 cells/dish) prepared from wild type and VGLUT1$^{-/-}$ mice, L-glutamate secretion were measured 20 min after stimulation with 1 mM ATP. (**E**) Secretion of bone degradation products from osteoclasts under the conditions in **A - C** were assessed fluorometrically after 20 min. The results are means ± SEM, n = 3.

Figure 7. mGluR-mediated regulation of the secretion of L-glutamate and fluorescent bone degradation products from RAW264.7 cells treated with RANKL. (**A**) Expression of mGluR8 gene as revealed by RT-PCR. (**B**) Expression of mGluR8 as revealed by immunoblotting (upper panel) and immunohistochemistry (lower panel). Bar = 10 μm. (**C**) RAW264.7 cells treated with RANKL (2.0×10^5 cells/dish) were incubated in the presence or absence of agonists or antagonists of glutamate receptors or DBcAMP as indicated and then stimulated with 50 mM KCl. The L-glutamate released after 20 min is shown. The results are means ± SEM, n = 3. Asterisks indicate statistically significant numbers (* $p < 0.01$, ** $p < 0.001$). (**D**) Fluorescent bone degradation products in the medium under the conditions in **A** were assessed fluorometrically. The results are means ± SEM, n = 3. Asterisks and marks indicate statistically significant numbers (* $p < 0.01$ compared with control, # $p < 0.001$ compared with + ACPT-I, † $p < 0.001$, compared with + L-Glutamate). (**E**) cAMP content in the osteoclast-like cells (2.0×10^5 cells/dish) under the conditions in **A**

were measured. The results are means ± SEM, n = 3. Asterisks and marks indicate statistically significant numbers (* $p < 0.01$ compared with control, # $p < 0.001$ compared with + ACPT-I, † $p < 0.001$, compared with + L-Glutamate). Additions: L-Glutamate, 0.5 mM; ACPT-I, 50 μM; CPPG, 100 μM; DBcAMP, 1 mM; (S)-3,5-DHPG, 10 μM; DCG-IV, 10 μM.

Figure 8. Inhibition of L-glutamate signal stimulated bone resorptive activity.
Osteoclasts were cultured on dentine slices in the absence (**A**) or presence (**B**) of 100 μM CPPG. In some experiments, 10 nM eel calcitonin was added (**C**). After 24 h, the resorption pits formed on the dentine slices were stained with Mayer's hematoxylin and quantified using the NIH Image program. The pictures of typical resorption pits formed on the dentine slices under respective condition are shown. (**D**) Ratio of resorption area to total area (pit area expressed in %) is shown. * $p < 0.01$, ** $P < 0.001$ compared with control. The results are means ± SEM, n = 6. Bar = 100 μm.

Figure 9. Microcomputed tomographs of female mouse femora from VGLUT1$^{+/+}$ and VGLUT1$^{-/-}$ mice. Microcomputed tomography 3D images of femoral metaphyses of VGLUT1$^{+/+}$ and VGLUT1$^{-/-}$ at the ages of 8 weeks (left) and 4 months (right) were constructed. The values of BV/TV are shown under each pictures.

Figure 10. Proposed L-glutamate signaling during bone resorption.
(left) Under the normal physiological conditions, a proportion of VGLUT1-containing small clear vesicles may fuse with the transcytotic vesicle. Upon stimulation with KCl or ATP, L-glutamate and bone degradation products are secreted through transcytosis. Then, the released L-glutamate acts as a negative feedback regulator through mGluR8-mediated signaling pathway, keeping osteoclasts in the suppressed state. (right) In osteoclasts of VGLUT1$^{-/-}$ mice, L-glutamate-mediated signaling pathway is impaired. This may induce

the desuppressive state of osteoclasts, causing stimulated bone resorption followed by osteoporosis. N, nucleus.

Supplemental Figure Legends

Figure S1. Immunohistochemical localization of VGLUT1 in osteoclasts prepared from bone marrow of wild type VGLUT1$^{+/+}$, VGLUT1$^{+/-}$ or VGLUT1$^{-/-}$. Expression of VGLUT1 or V-ATPase subunit A was detected by indirect immunofluorescence microscopy. Data with control IgG were also shown as a negative control. Expression of VGLUT1 in cerebral cortex of these mice was also shown as another control. Bar = 50 μm.

Figure S2. Localization of VGLUT1 in osteoclasts grown on bone pieces was examined by double-labeling immunofluorescence microscopy. The staining pairs were as follows: VGLUT1 and Lamp 2 (A), VGLUT1 and TGN38 (B), VGLUT1 and GM130 (C), VGLUT1 and transferrin receptor (TfR) (D). The immunological localization was observed under a confocal microscope. A horizontal view of a merged picture is also shown. Bar = 10 μm.

Figure S3. Expression of mGluRs genes other than mGluR8 in osteoclasts.
Results of RT-PCR analysis of total cellular RNA were shown. Expression of genes of the indicated mGluR isoform in brain (lanes 1 and 4, as control), RAW264.7 cells (lanes 2 and 5), RAW264.7 cells treated with RANKL (lanes 3 and 6), and osteoclasts (lanes 7 and 8) were shown. The PCR products were not detected if reverse transcriptase is omitted from the reaction mixture (-RT) (lanes 4-6 and 8). The G3PDH transcript, as a loading control, is also shown.

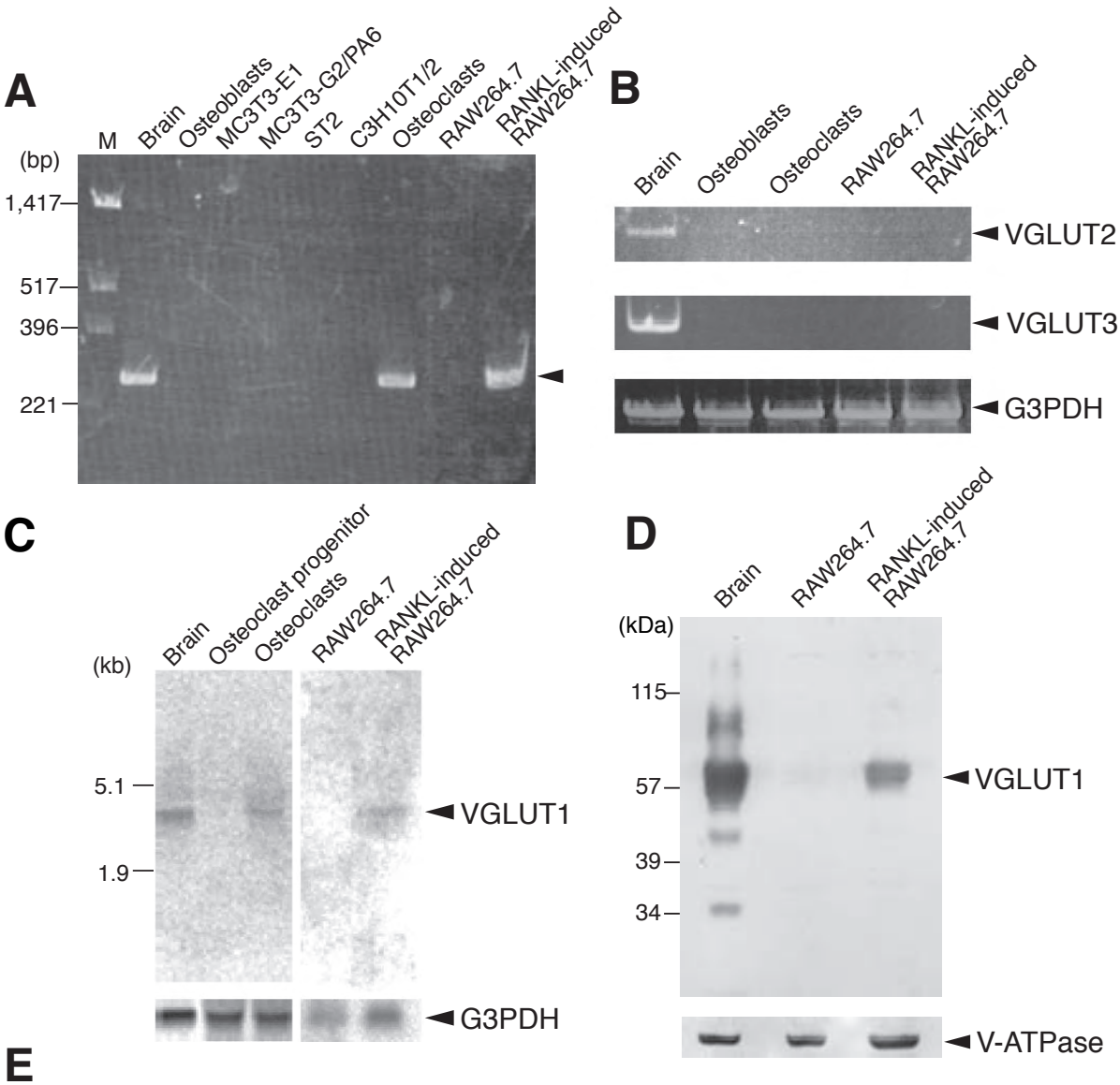

Figure 1
Morimoto, R et al.

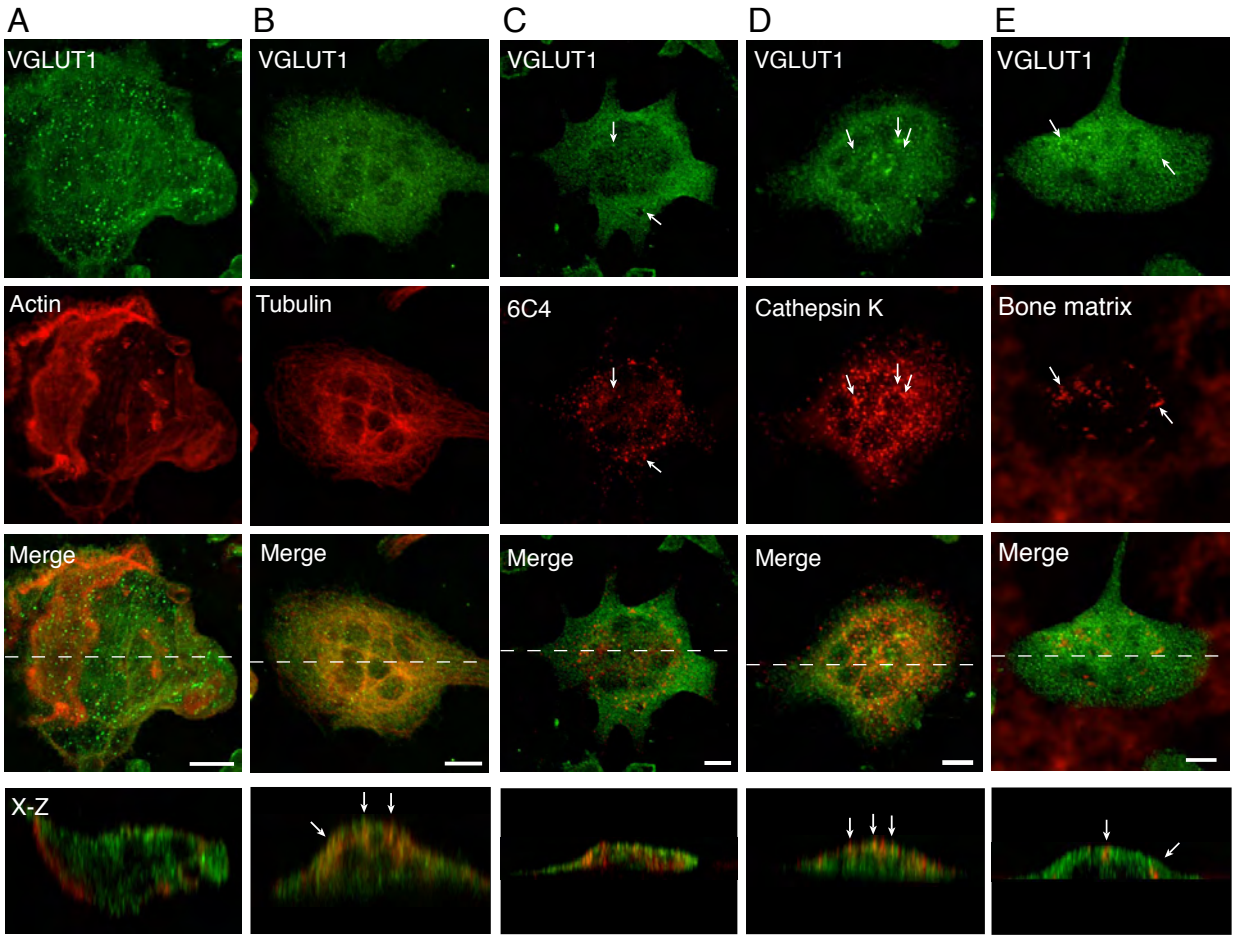

Figure 2
Morimoto, R et al.

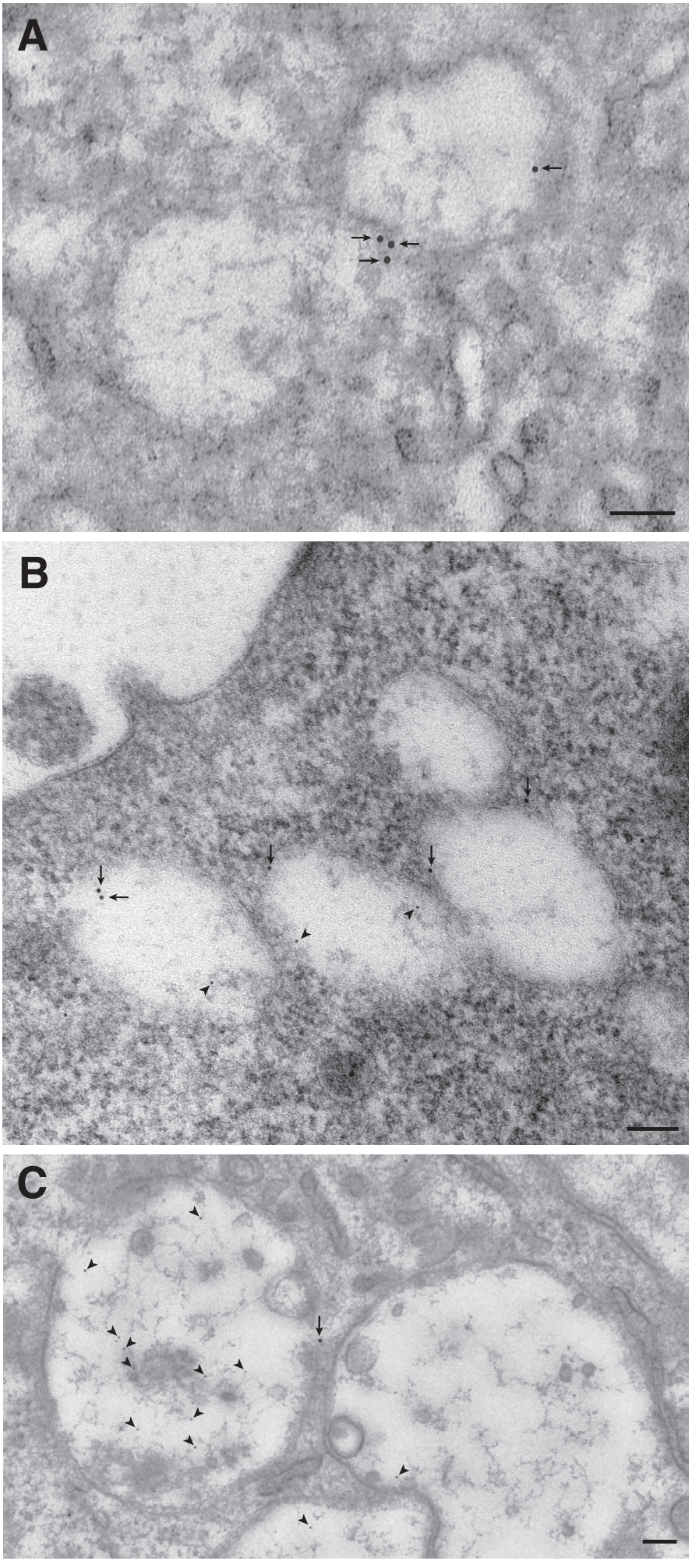

Figure 3
Morimoto, R et al.

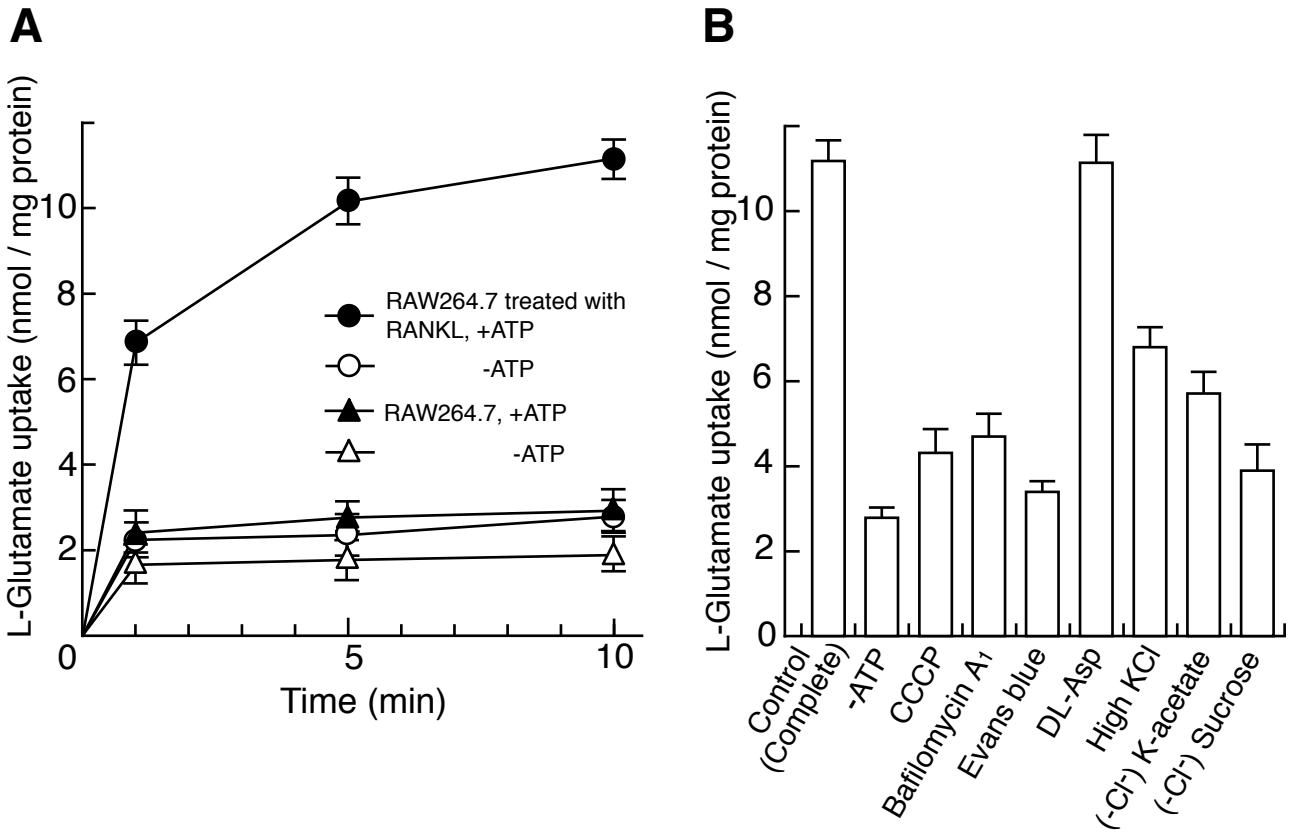

Figure 4
Morimoto, R et al.

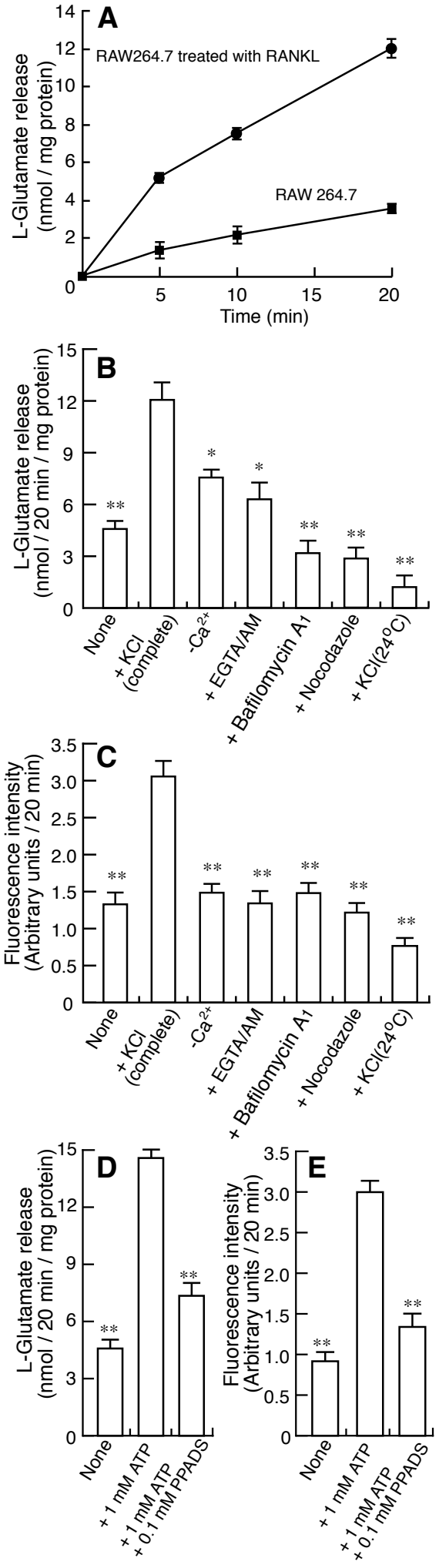

Figure 5
Morimoto, R et al.

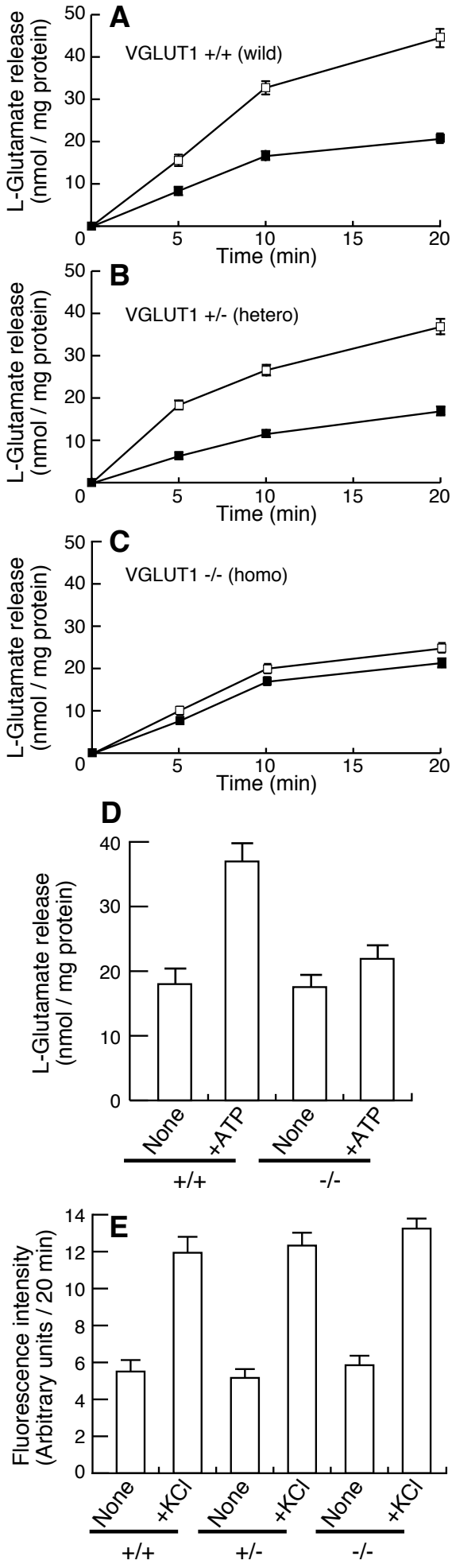

Figure 6
Morimoto, R et al.

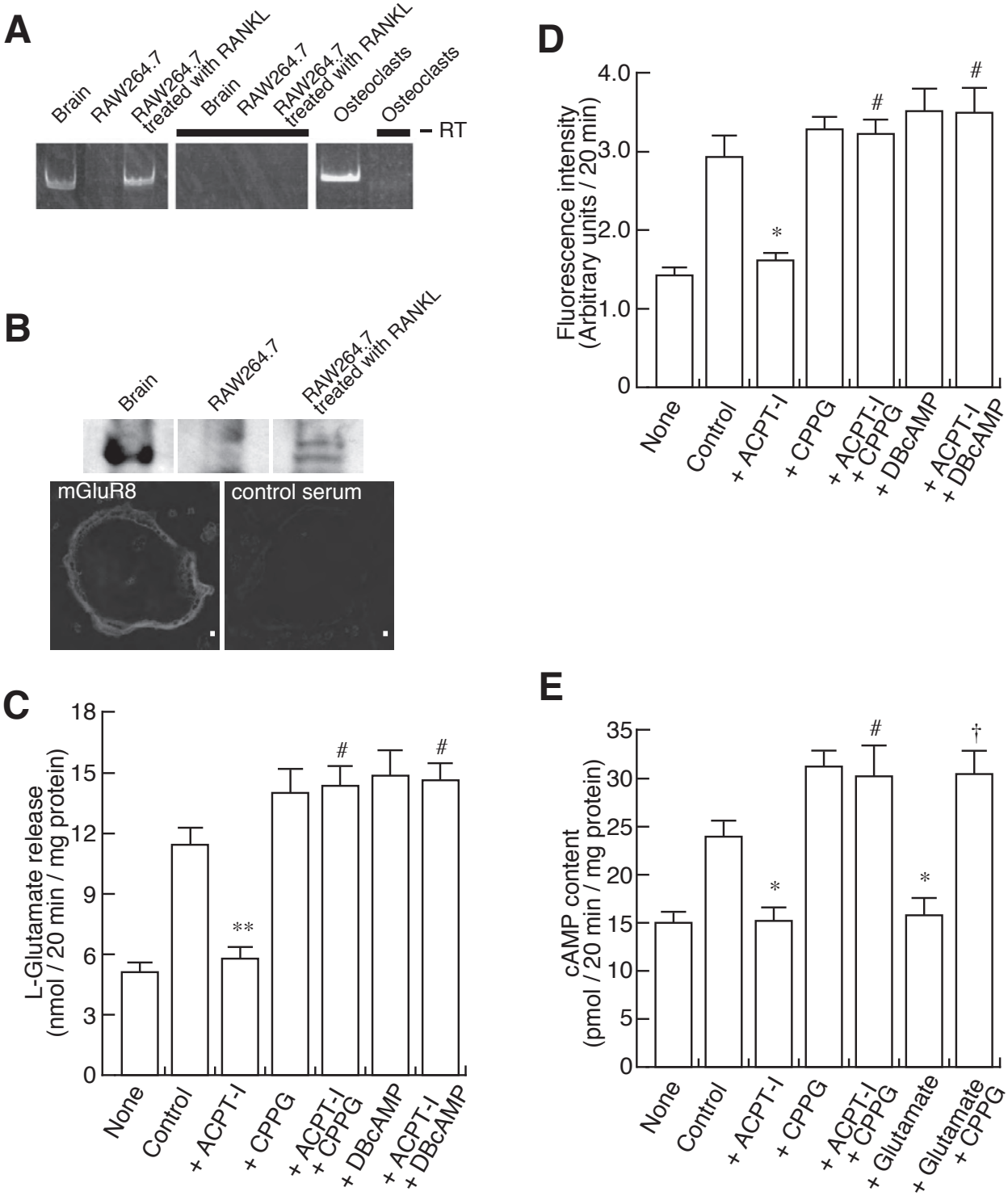

Figure 7
Morimoto, R et al.

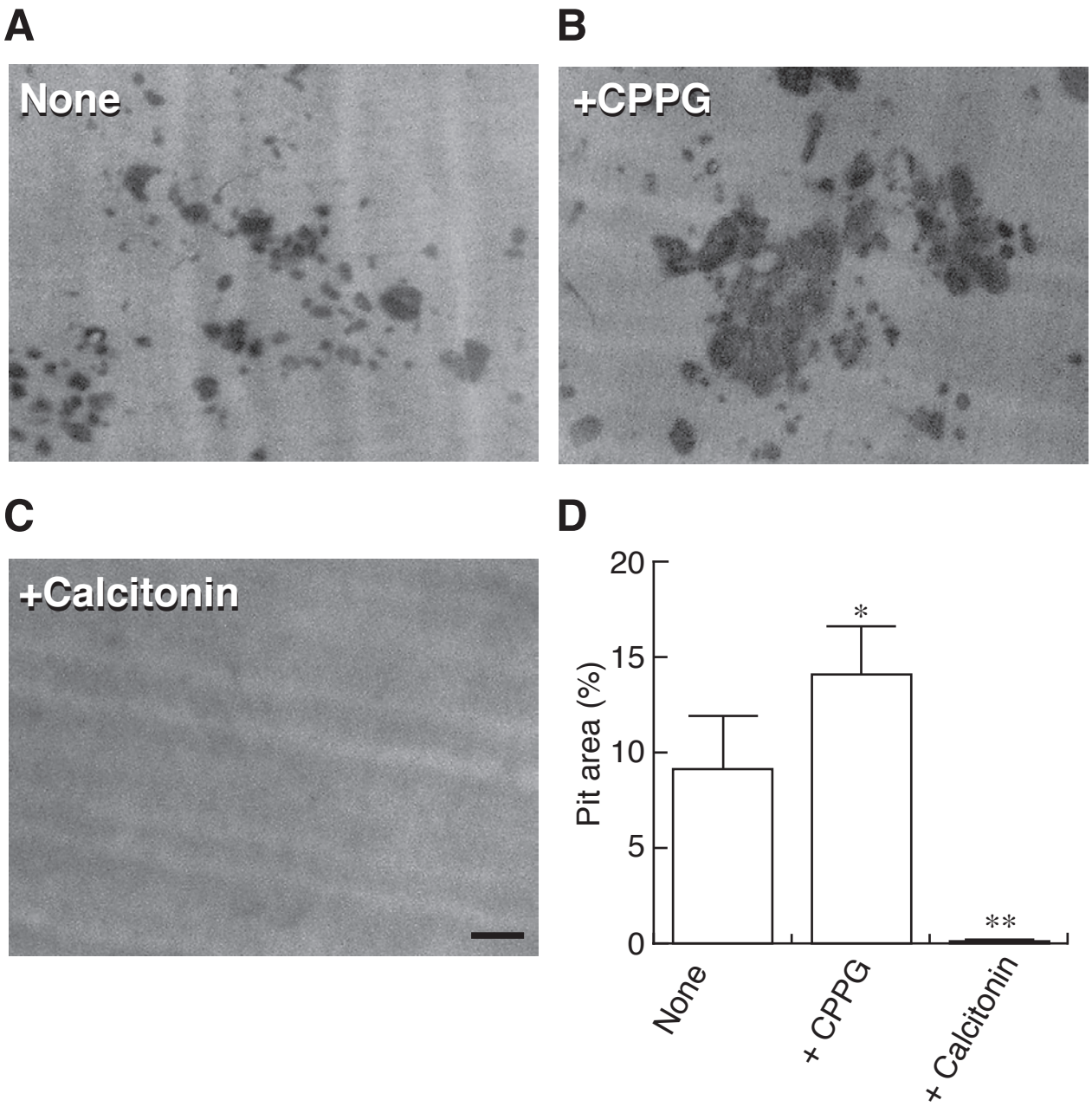

Figure 8
Morimoto, R et al.

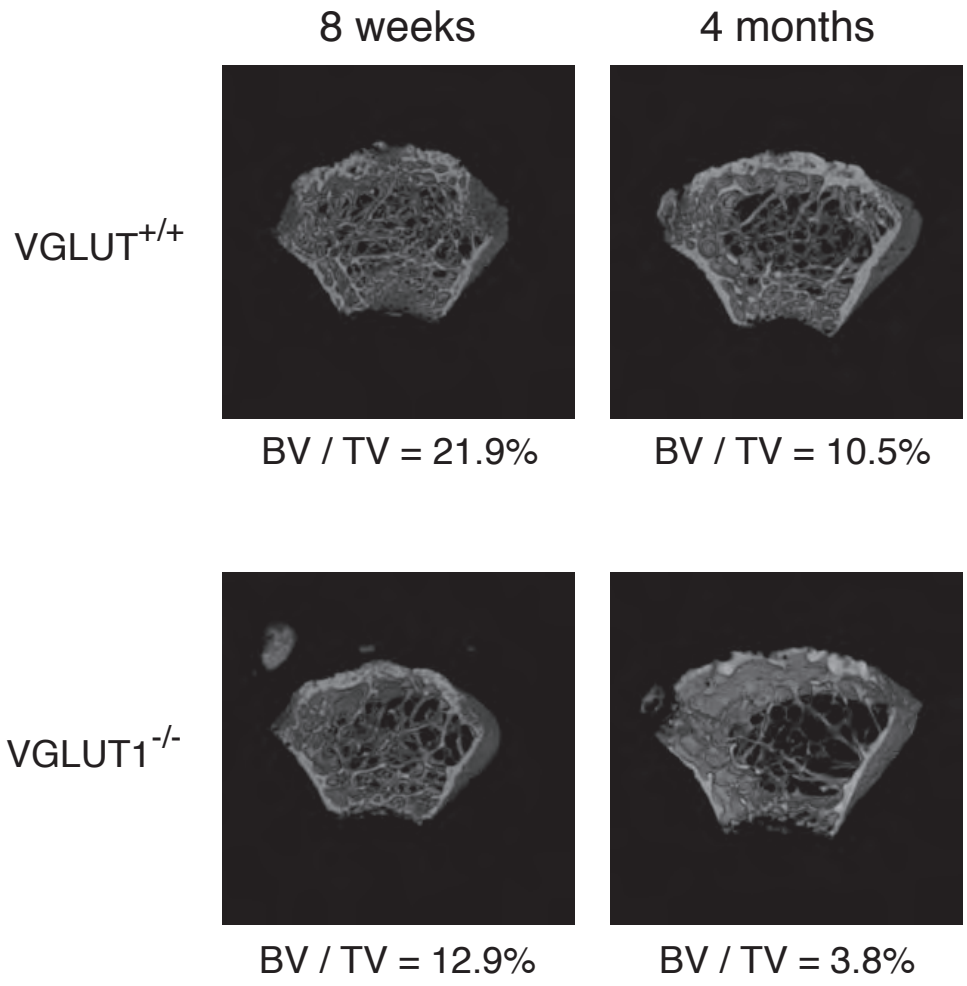

Figure 9
Morimoto, R et al.

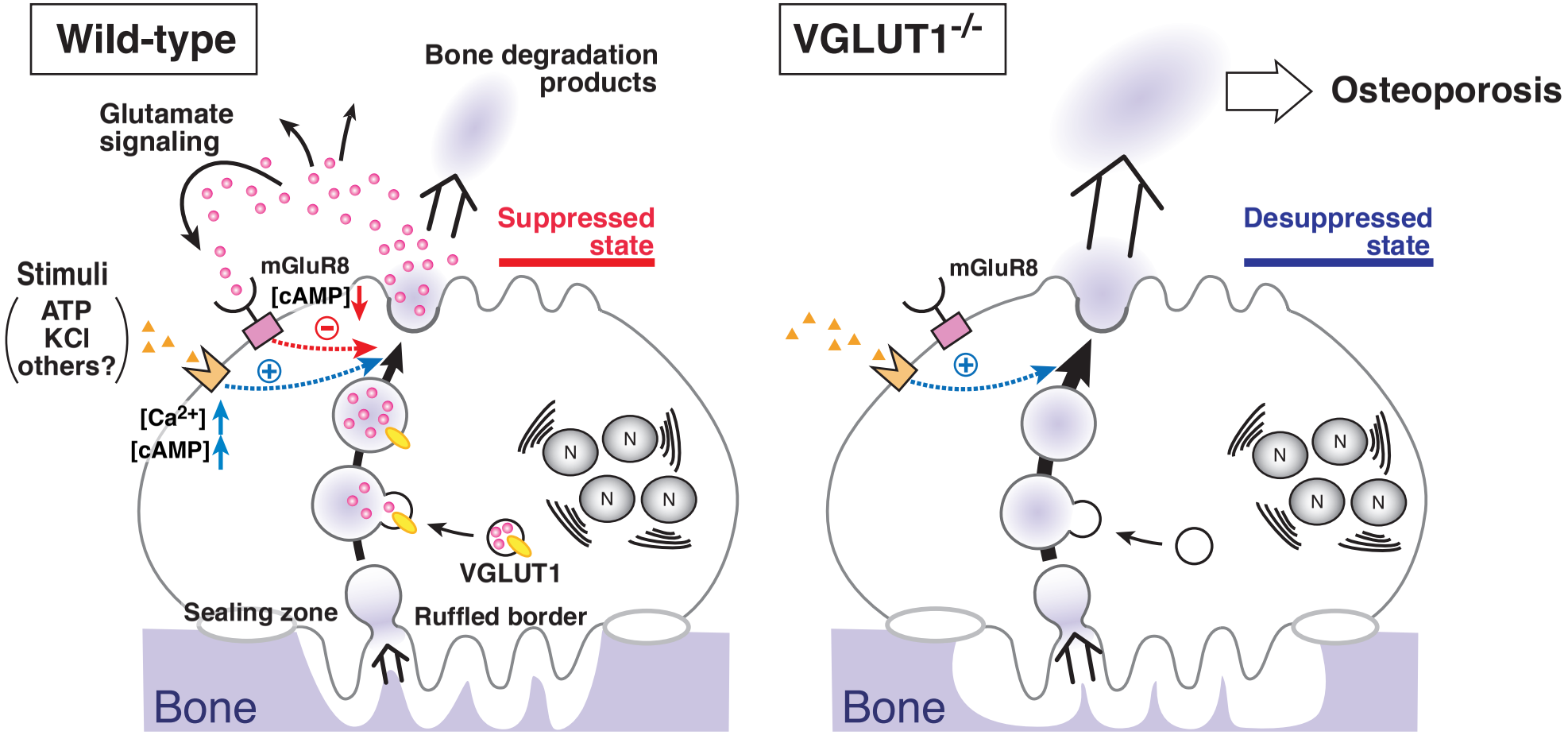

Figure 10
Morimoto, R et al.

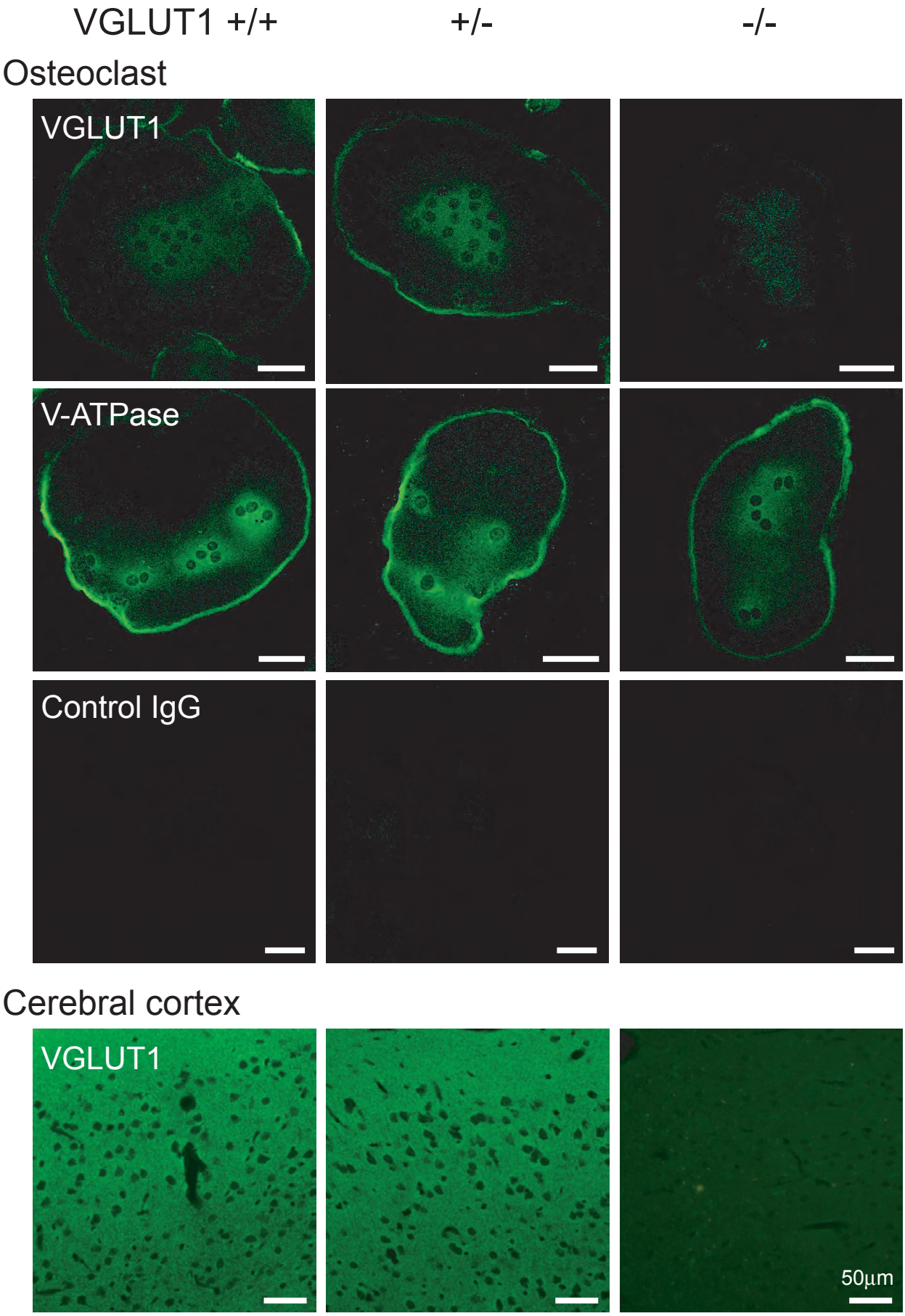

Supplementary Information
Figure S1
Morimoto, R et al.

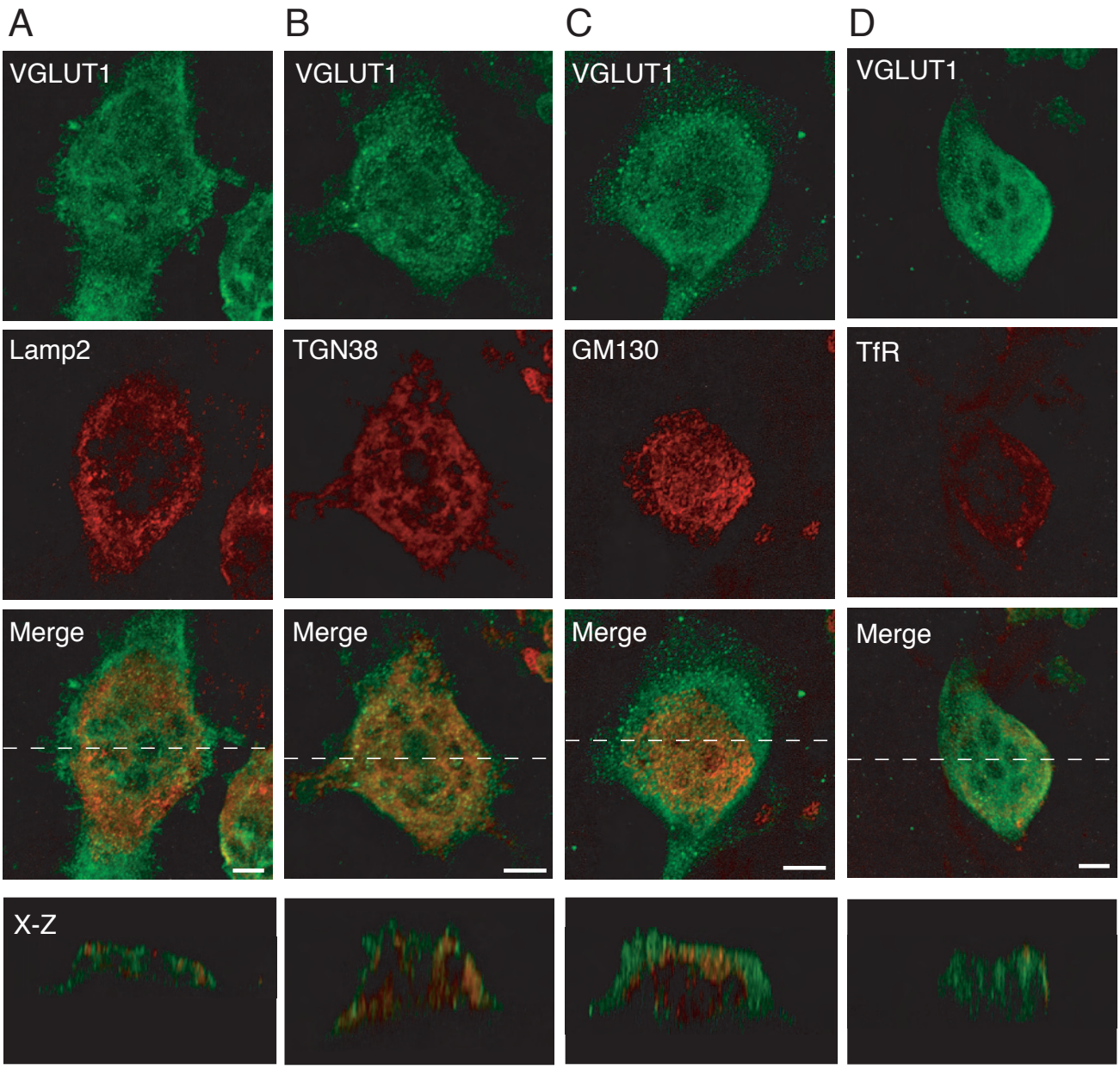

Supplementary Information
Figure S2
Morimoto, R et al.

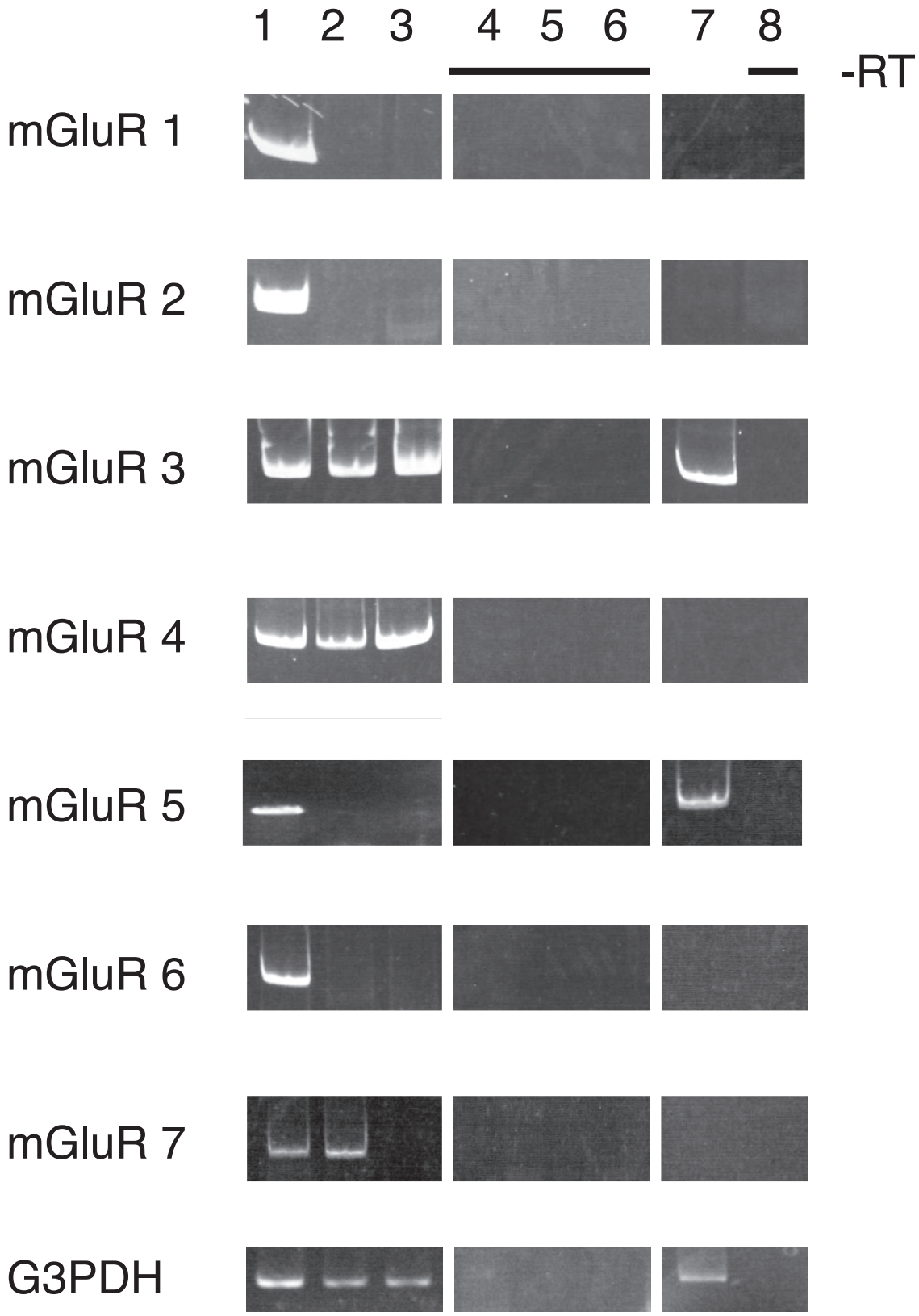

Supplementary Information
Figure S3
Morimoto, R et al.

PCR primers used for detection of different VGLUTs and mGluRs.

name	size	primer sequences	Tm (°C)	Genbank No.
VGLUT1	335bp	1687 5'-- AGTGAAATGGAAGACGAGGTT --3' 1707 2002 5'-- TTCGGCACGAGCTTGAAACT --3' 2021	56°C	U07609
VGLUT2	627bp	1874 5'-- CATCTCCTTCTTCGTGCTT --3' 1892 2480 5'-- GACTTGCTTGGTTGATATGTT --3' 2500	56°C	AF324864
VGLUT3	330bp	74 5'-- AGGAAGGAGTGAAGAATCCCG --3' 94 383 5'-- GTTTCCCATCCACATACACAG --3' 403	56°C	AF510321
mGluR1	207bp	1155 5'-- AAATCTACAGCAATGCTGGCGA --3' 1176 1340 5'-- CTTCGATGACTTCATCTCTGTC --3' 1361	55°C	M61099
mGluR2	301bp	1091 5'-- CCACTCTCTGCGGGCCGTGCC --3' 1112 1369 5'-- CCTATCTGCGGGCAGGCAGTGGG --3' 1391	64°C	M92075
mGluR3	396bp	746 5'-- GCTCCAACATCCGCAAGTCCTA --3' 767 1120 5'-- GACAAGCACCTGGCCATTGACA --3' 1141	59°C	M92076
mGluR4	373bp	2023 5'-- TGTTCGCTCCGCCGCATCTTCCTA --3' 2046 2372 5'-- TCTCGGGTCTTGATGGCGTACACAG --3' 2395	64°C	M92077
mGluR5	514bp	1254 5'-- GTCTCCTGATGTCAAGTGGTT --3' 1274 1747 5'-- GGACCACACTTCGTCATCATC --3' 1767	56°C	D10891
mGluR6	338bp	324 5'-- CTGAAGAAAGAGCAAGGCGTG --3' 344 640 5'-- ATCTGGGGTATCGCAAACAGGC --3' 661	50°C	D13963
mGluR7	416bp	1415 5'-- AGGGCAACCGTGGAAGGATTTG --3' 1436 1810 5'-- TCATAACGCCCTGGAGCATCG --3' 1830	60°C	D16817
mGluR8	400bp	482 5'-- CCATATTCACCAAGCCCGACAAG --3' 504 861 5'-- GTCTCCAGCAGGCGTTTGATA --3' 881	59°C	U63288

Supplementary Table SI
Morimoto, R et al.